

Quantum spin chains with multiple dynamics

Xiao Chen,¹ Eduardo Fradkin,² and William Witczak-Krempa³

¹*Kavli Institute for Theoretical Physics, University of California at Santa Barbara, CA 93106, USA*

²*Department of Physics and Institute for Condensed Matter Theory,*

University of Illinois at Urbana-Champaign, 1110 West Green Street, Urbana, Illinois 61801-3080, USA

³*Département de physique, Université de Montréal, Montréal (Québec), H3C 3J7, Canada*

(Dated: November 9, 2017)

Many-body systems with multiple emergent time scales arise in various contexts, including classical critical systems, correlated quantum materials, and ultra-cold atoms. We investigate such non-trivial quantum dynamics in a new setting: a spin-1 bilinear-biquadratic chain. It has a solvable entangled groundstate, but a gapless excitation spectrum that is poorly understood. By using large-scale DMRG simulations, we find that the lowest excitations have a dynamical exponent z that varies from 2 to 3.2 as we vary a coupling in the Hamiltonian. We find an additional gapless mode with a continuously varying exponent $2 \leq z < 2.7$, which establishes the presence of multiple dynamics. In order to explain these striking properties, we construct a continuum wavefunction for the groundstate, which correctly describes the correlations and entanglement properties. We also give a continuum parent Hamiltonian, but show that additional ingredients are needed to capture the excitations of the chain. By using an exact mapping to the *non-equilibrium* dynamics of a classical spin chain, we find that the large dynamical exponent is due to subdiffusive spin motion. Finally, we discuss the connections to other spin chains and to a family of quantum critical models in 2d.

It is common for many-body quantum systems to possess multiple time-scales that determine the low-energy dynamics. In a gapless system, the dynamics will be characterized by the dispersion relation of the excited states (quasiparticles need not exist), $E = Ak^z$, where k is the wavevector of the mode and z the dynamical exponent. Different modes can have different z exponents. For instance, a metal near a quantum critical point can have different dispersions for the electrons and the various order parameter fluctuations [1–6]. However, this phenomenon has been far less studied in other types of systems. Many studies have examined simpler systems, such as models described by relativistic conformal field theories having $z = 1$, which enjoy additional symmetries that constrain the dynamics [3, 7, 8].

In this work, we reveal multiple dynamical exponents in a new setting: a strongly correlated 1d spin system. Further, these exponents will be shown to vary continuously as a function of a coupling in the Hamiltonian. The spin 1 quantum spin chain in question is a generalization of the so-called Motzkin Hamiltonian introduced by Bravyi *et al* [9]. Its groundstate can be determined exactly but not its excitation spectrum. With the help of large-scale Density Matrix Renormalization Group (DMRG) simulations, we discover low lying excitations with different dynamical exponents. In order to gain insight in the low-lying spectrum we determine a continuum version of the groundstate, and find a parent Hamiltonian. The latter possesses an excitation spectrum that is distinct from the spin chain but can provide useful insight into the construction of the full low energy field theory. This illustrates how a given groundstate can have starkly different excitations, and offers some guidance in the construction of the true low-energy description of the chain. Owing to the Rokhsar-Kivelson [10]

(RK) structure of the spin Hamiltonian, we are able to connect the problem of determining the excitation spectrum to studying the *non-equilibrium* dynamics of the corresponding classical 1d chain [11]. This sheds light on the subdiffusive nature ($z > 2$) of the excitations observed with DMRG. Finally, we provide connections to a family of two dimensional quantum critical system that have conformally invariant wavefunctions [12, 13].

Critical quantum spin chain. The Hamiltonian describes N $S = 1$ spins interacting via nearest neighbor exchange:

$$H_{\text{bulk}} = \sum_{i=1}^{N-1} |D\rangle_{i,i+1}\langle D| + |U\rangle_{i,i+1}\langle U| + c|V\rangle_{i,i+1}\langle V| \quad (1)$$

where $|D\rangle\sqrt{2} = |0d\rangle - |d0\rangle$, $|U\rangle\sqrt{2} = |0u\rangle - |u0\rangle$, $|V\rangle\sqrt{2} = |00\rangle - |ud\rangle$; $c \geq 0$ is a free parameter. Here, $u, d, 0$ label the S^z eigenstates. In terms of the spin operators $S^{x,y,z}$, Eq.(1) takes the form of an anisotropic bilinear-biquadratic Hamiltonian $\sum_i (A_{ab}S_i^a S_{i+1}^b + B_{abcd}S_i^a S_i^b S_{i+1}^c S_{i+1}^d)$; we give the coefficients A, B in Supplemental Material [14]. We will work with open chains with an additional boundary term

$$H = H_{\text{bulk}} + \frac{1}{2}S_1^z(S_1^z - 1) + \frac{1}{2}S_N^z(S_N^z + 1) \quad (2)$$

H has a global U(1) symmetry generated by $S_{\text{tot}}^z = \sum_i S_i^z$ [15]. When $c = 1$, H reduces to the so-called Motzkin Hamiltonian [9]. In that case, the groundstate is the equal weight superposition of all states corresponding to Motzkin paths. For $N=3$:

$$|\mathcal{M}_3\rangle = \frac{1}{\sqrt{4}}(|\underline{\underline{\underline{\quad}}}\rangle + |\underline{\underline{\swarrow}}\rangle + |\swarrow\underline{\underline{\quad}}\rangle + |\swarrow\underline{\swarrow}\rangle) \quad (3)$$

with the notation $u = \swarrow$, $d = \searrow$, $0 = \underline{\underline{\quad}}$. This al-

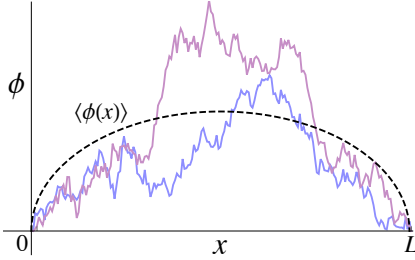


FIG. 1. Representation of 2 Motzkin paths via the height variable ϕ . Each path can be interpreted as a Brownian excursion. The dashed line is the average of ϕ in the groundstate (4). The spin $\langle S^z \rangle = \langle \partial_x \phi \rangle$ tends to zero deep in the bulk.

lows for the height representation [9, 15–17] shown in (3) and in Fig. 1: the height variable ϕ_i is pinned to zero at both ends, $\phi_0 = \phi_N = 0$, while for $i \geq 1$ we have $S_i^z = \phi_i - \phi_{i-1}$. In this language, a Motzkin path has $\phi_i \geq 0$ while being pinned to zero at the extremities. By virtue of being an equal weight superposition, the Motzkin groundstate $|\mathcal{M}_N\rangle$ is annihilated by all 3 projectors in Eq.(1). It is thus a groundstate when $c \geq 0$. At $c = 1$, it was shown to be the unique groundstate as a consequence of the boundary term, a fact which remains true as long as $c > 0$ [9]. At the special point $c = 0$, other states belong to the groundstate manifold such as the all-0 product state.

Groundstate in the continuum. In the continuum limit where x spans distances much larger than the lattice spacing, the groundstate wavefunction of the Motzkin Hamiltonian (2) takes the simple form

$$\Psi_0[\phi(x)] = \frac{1}{\sqrt{Z}} e^{-\frac{\kappa}{2} \int_0^L dx (\partial_x \phi)^2} \prod_x \theta(\phi(x)) \quad (4)$$

which is defined in terms of the (coarse-grained) height field ϕ introduced above. This is reminiscent of the wavefunction of the quantum Lifshitz model in 2d [12, 18], with the distinction that ϕ here is non-compact. We discuss further connections between these models in the Outlook. To match the boundary conditions of the lattice wavefunction, we impose the Dirichlet condition $\phi(0) = \phi(L) = 0$ for a chain of length L . In this language, the spin field is given in the continuum by $S^z = d\phi/dx$; κ is a parameter whose value will be fixed later and $\theta(\phi)$ is the Heaviside function that enforces ϕ to be non-negative. This constraint is necessary to obtain the Motzkin state (see Eq.(3)). The normalization factor Z takes the form of a (0+1)-dimensional partition function:

$$Z = \int_{\phi(0)=\phi(L)=0} \mathcal{D}\phi(x) e^{-\kappa \int_0^L dx (\partial_x \phi)^2} \prod_x \theta(\phi(x)) \quad (5)$$

The exponential term in the wavefunction (4), which determines the probability of a path $\phi(x)$, can be understood by mapping the problem to a random walk [9]. Let us momentarily go back to the lattice, which means that

we need to consider discrete Brownian motion in 1d restricted to the *non-negative* integers $\phi_i \geq 0$. Taking the horizontal axis of the path i as the time direction, the random walk can be illustrated as follows. The walker takes a step chosen out of the 3 options: 1) move up by one, 2) move down by one, 3) stay at the same place. The walk is subject to the constraint $\phi_i \geq 0$, and it must start/end at the same point, $\phi = 0$, but is otherwise random. This process is called a Brownian excursion, and is illustrated in Fig. 1. Any valid path constructed out of a succession of such steps has the same probability, whose value is given by the Motzkin wavefunction squared $P[\phi_i] = |\langle \phi_i | \mathcal{M}_N \rangle|^2$. P thus equals the inverse of the total number of Motzkin paths. Taking the long time limit, the random walk is described by a Langevin equation for the continuum field $\phi(x) \geq 0$. Statistical physics [19] then tells us that the probability of a given path is given by the amplitude squared $|\Psi_0[\phi(x)]|^2$ of our wavefunction (4). For the Motzkin type random walk, the variance at a typical step is $\sigma^2 = \frac{1}{3}(1^2 + 0^2 + (-1)^2) = 2/3$. This determines the diffusion constant in the long time limit, $1/(4\kappa) = \sigma^2/2 = 1/3$, i.e. $\kappa = 3/4$. Equipped with our parameter-free wavefunction, we can compute properties of the groundstate in the continuum limit. By comparing these properties with that for the discrete groundstate, we can show that Eq.(4) and the groundstate for Eq.(2) are exactly the same in the thermodynamical limit. For instance, the expectation value of the spin is $\langle S^z(x) \rangle = \langle \partial_x \phi \rangle = (L - 2x)/\sqrt{\pi\kappa L(L - x)x}$, which changes sign going from the left to the right end, see Fig. 1. The non-zero expectation value arises due to the boundary conditions. Indeed, deep in the bulk $\langle S^z(\frac{L}{2} + a) \rangle \propto a/L^{3/2}$ rapidly vanishes as $L \rightarrow \infty$ at fixed a . This matches the calculation using the lattice wavefunction [9, 15, 20].

The Motzkin groundstate is highly entangled in the sense that the Rényi entanglement entropy (EE) has a logarithmic scaling with subsystem size [9, 15]. By considering the subregion A to be the interval $[0, L_A]$, we find using (4):

$$S_n = \frac{1}{2} \ln \left(\frac{L_A(L - L_A)}{\epsilon L} \right) + b(n) \quad (6)$$

where the logarithm's prefactor is independent of the Rényi index n and of κ ; ϵ is a short-distance cutoff. The constant $b(n)$ depends on n, κ , and when we fix $\kappa = 3/4$ we find an exact agreement with the lattice calculation [9, 15]. The calculation of Eq.(6) is greatly simplified by the special form of the wavefunction Eq.(4), allowing us to adapt the methods of [21], described in the Supplemental Material [14]. Although in the limit $L_A \ll L$, the EE scales as $\frac{1}{2} \ln L_A$, the complete form of the EE is distinct from what is found in CFTs, and implies that the long-distance limit of the chain is not described by a CFT [9]. If we take region A to be an interval located deep inside the bulk, we find $S_n = \frac{1}{2} \ln \frac{L_A}{\epsilon}$.

The Motzkin wavefunction shows other clear differ-

ences from the groundstate of a CFT, and is in fact less entangled. This can be seen by studying the mutual information for 2 disjoint intervals A, B , which was not studied before. The mutual information is defined as $I(A, B) = S(A) + S(B) - S(A \cup B)$. It measures the quantum correlations between A and B , giving an upper bound for two-point correlation functions of local observables [22]. In the wavefunction (4), for 2 disjoint intervals deep inside the bulk, we find $I(A, B) = 0 + O(L_A L_B / L^2)$ [14]. This is consistent with the result for the spin 2-point function: $\langle S^z(x_1) S^z(x_2) \rangle = 0$ if $x_1 \neq x_2$ in the Motzkin wavefunction [15], which can be readily derived using our continuum wavefunction [23]. The vanishing of $I(A, B)$ can be understood by using the above mapping between the wavefunction (4) and the random walk problem. Deep inside the bulk, we can ignore the boundary conditions and remove the constraint $\phi > 0$ due to the exponentially small probability for ϕ being near zero in (4). In this regime the random walk reduces to regular Brownian motion, instead of the constrained Brownian excursion. Therefore, the probability for a walker moving a distance $\delta\phi$ in “time” δx is independent of the history. There are essentially no correlations between the 2 disjoint intervals and we expect that the mutual information between them in the quantum state vanishes. This stands in contrast with CFTs, for which the mutual information between two well-separated small intervals with distance r scales as $1/r^\Delta$, with Δ determined by the scaling dimension of primary operators [24].

The fact that the EE of a single interval diverges logarithmically but the mutual information between 2 intervals vanishes, suggests that non-local degrees of freedom are responsible for the entanglement measured via the EE. These escape the more “local” 2-interval measures.

A field theory with the Motzkin groundstate. We now take a step further and construct one quantum field theory whose groundstate is (4), and has $z \neq 1$. The Hamiltonian of the field theory reads

$$H_{\text{orb}} = \int dx \left(\frac{1}{2} \Pi^2 + \frac{\kappa^2}{2} (\partial_x^2 \phi)^2 + V(\phi) \right) \quad (7)$$

Π is the canonical conjugate to the height operator ϕ . $V(\phi)$ is the potential that enforces the constraint $\phi \geq 0$: $V(\phi < 0) = \infty$ and is zero otherwise. Thus, the target space of ϕ is the positive half-line, i.e. the orbifold obtained by moding the real line by the transformation $\phi \rightarrow -\phi$. To show that (4) is the groundstate of H_{orb} , we can rewrite the latter as $H_{\text{orb}} = \int_x (Q^\dagger(x) Q(x) + V(\phi))$, where we have subtracted an infinite groundstate energy and defined the annihilation operator [12, 18] $Q(x) = \frac{1}{\sqrt{2}} (\frac{\delta}{\delta \phi} - \kappa \partial_x^2 \phi)$. The groundstate of Eq.(7) is annihilated by Q . This defines a functional equation that is satisfied by Eq.(4): $Q\Psi_0[\phi] = 0$.

Since $\Pi = \partial_t \phi$, we see that Eq.(7) is invariant under the spacetime dilation $x \rightarrow \lambda x$ and $t \rightarrow \lambda^2 t$ (with an appropriate field rescaling), implying that this Hamiltonian has dynamical exponent $z = 2$ and is thus not a CFT, in

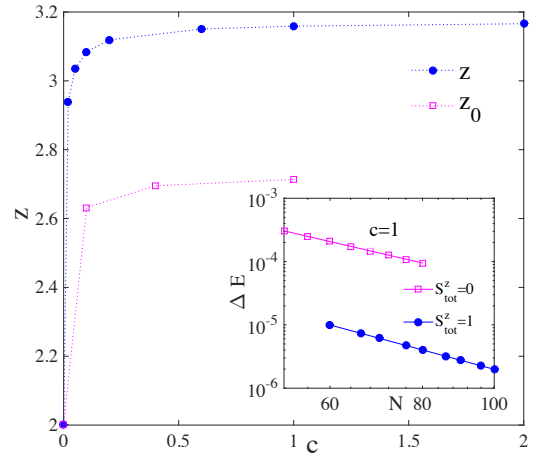


FIG. 2. DMRG data for the dynamical exponent of the generalized Motzkin Hamiltonian Eq.(2) versus the coupling c . The blue circles give z for the lowest excitation, which has $S_{\text{tot}}^z = 1$. The pink squares give z_0 for the lowest excitation in the $S_{\text{tot}}^z = 0$ sector. **Inset:** log-log plot of the energy gap versus system size N used to extract z via $\Delta E \propto 1/N^z$.

agreement with the EE results above. Now, H_{orb} and the continuum limit of the Motzkin Hamiltonian share the same groundstate, but do they have the same low energy excitations? To answer this question, we now investigate the excited states of Motzkin Hamiltonian Eq.(2). Because the problem is not readily amenable to analytical calculations, we turn to DMRG simulations.

DMRG & dynamical exponents. At $c = 1$, the many-body gap was shown to scale as $1/N^z$, with the analytical bound $z \geq 2$ [16, 25], suggesting that our above field theory is a viable candidate to describe the Motzkin Hamiltonian. However, exact diagonalization (ED) [9] on small systems yielded $z = 2.91$, while previous DMRG calculations [20] yielded $z = 2.7 \pm 0.1$. As we shall see, the former result suffers from strong finite size effects, while the latter does not correspond to the true lowest excited state. In order to understand the spectrum, we have performed large-scale DMRG calculations using the ITensor library, which we benchmarked using ED for short chains [14]. The results for z as a function of c are shown in Fig. 2. At $c = 1$, we find $z = 3.16$ by using chains of length up to $N = 100$, an exponent substantially larger than the numerical results quoted above. The excitation associated with this dynamical exponent is two-fold degenerate, with the 2 states having quantum numbers $S_{\text{tot}}^z = \pm 1$, respectively. Interestingly, we also found a singly-degenerate excited state with higher energy in the $S_{\text{tot}}^z = 0$ sector; it has dynamical exponent $z_0 = 2.71 < z$. The proximity of z_0 to the previous DMRG result [20] suggests that these authors worked in the $S_{\text{tot}}^z = 0$ sector, thus missing the lowest excitations. We have also analyzed the excitations in the $S_{\text{tot}}^z = 2$ sector and have found that they have the same dynamical exponent as in the $S_{\text{tot}}^z = 1$ sector [14].

As we tune c away from 1, the groundstate is still annihilated by all the local interaction terms, as is the case in (2) [9]. We find that H remains gapless but that the dynamical exponent z varies continuously with c . Fig. 2 shows that z decreases monotonically as c decreases, and $z > 2$ except when $c = 0$. Our DMRG results thus rule out the field theory above as the correct low energy description of H for $c > 0$. Interestingly, it provides a concrete instance where different Hamiltonians, here the generalized Motzkin Hamiltonian Eq.(2) and H_{orb} Eq.(7), can have the same groundstate but markedly distinct excitations. At the special point $c = 0$, H has $z = 2$ by virtue to a mapping to the ferromagnetic Heisenberg spin-1/2 chain [9]. In that case, the groundstate manifold becomes highly degenerate, growing exponentially with N , and contains the all-zero product state. We can construct an exact excited state in the form of a spin wave. Since we are interested in the thermodynamic limit, we can work with an infinitely long chain, in which case the excited state reads: $\sum_j e^{ikj} |u_j\rangle |0\rangle_{\text{rest}}$, where k specifies the wave number of the mode. The wave has $S_{\text{tot}}^z = 1$ and energy $1 - \cos k$, leading to $z = 2$ at small k .

We now provide physical insight into the result $z > 2$ observed when $c > 0$. Earlier we have seen how the groundstate properties of the generalized Motzkin Hamiltonian map to the classical Brownian motion of a particle. We can go further and study the *full spectrum* of the Hamiltonian of Eq.(2) by examining the non-equilibrium dynamics of a *classical* 1d spin chain. Indeed, the RK form of H ensures that we can map the quantum spin chain problem to the dynamics of classical chain governed by a Markovian master equation [11, 26, 27]. The non-diagonal elements of the rate matrix W are given by the matrix elements of H between spin configurations, $W_{C,C'} = -\langle C|H|C'\rangle$; the diagonal elements of W follow from detailed balance. The quantum dynamics of (2) thus maps to the critical slowing down of the corresponding classical model endowed with dynamics W .

Hohenberg and Halperin have classified the critical slowing down of classical critical models according to the symmetries of the low energy modes [28]. For instance, the Glauber dynamics of an Ising chain belongs to Model A because single spin flips (non-conserving) processes are allowed. In this case, the motion of a domain wall is described by the diffusion equation yielding a dynamical exponent $z = 2$ [28]. In contrast, the generalized Motzkin Hamiltonian (2) maps to classical dynamics described by the Model B universality class since the spin flipping processes preserve S_{tot}^z . The conservation law constrains the spin flips and can thus slow down the dynamics, leading to a larger z [13, 29]. For instance, the spin-conserving Kawasaki dynamics of an Ising chain show $z \approx 3$ in a certain temperature range [29, 30]. In Fig. 2, we also observe such subdiffusive behavior with $z \approx 3$. To understand such behavior, it is useful to analyze the physics near $c = 0$, where we have shown above that $z = 2$ results from the diffusive motion of an up spin in a sea of 0s. As we turn on $c > 0$, the $|V\rangle\langle V|$ projector in Eq.(1)

generates more ud pairs, which slow down the motion of the up spin. Indeed, imagine we create an ud pair next to an u spin, $0uud0$. Using the projectors in Eq.(1), it takes 3 moves to translate the leftmost u one site to the right, as opposed to 1 move in the absence of the ud pair. This argument suggests that the dynamics slow down as c increases, in agreement with our DMRG results Fig. 2, but doesn't explain the specific change of z with c , nor the presence of excitations with different dynamical exponents. One can get quantitative results for z by performing Monte Carlo sampling of the non-equilibrium classical spin chain, as we mention below. Finally, it would be desirable to obtain a field theory description for the full spectrum. We expect that marginal operators play a key role in explaining the change of the dynamical exponents with c .

Summary & outlook. We have studied the intricate dynamics of a $S = 1$ quantum spin chain, Eq.(2). Our DMRG simulations have revealed that the gapless system has a dynamical exponent z that changes as a function of a coupling c in the Hamiltonian, Fig. 2. Interestingly, similar behavior was observed in quantum critical lattice models in 2 spatial dimensions [13], where the Hamiltonian also takes a RK form. These authors used the mapping to the non-equilibrium dynamics of a classical model described above in order to determine z via classical Monte Carlo simulations; dynamics with a varying $z > 2$ were also observed. It would be interesting to analyze these 2d Hamiltonians further to see if an additional excitation with a smaller z appears, just as in our case. The Monte Carlo methods could also be applied in our case to reach bigger system sizes. A further connection is that the 2d groundstates studied in [13] have an emergent *spatial* conformal symmetry [12, 13, 18], a feature that also arises in the generalized Motzkin model, although in a more subtle way [23]. We should also note that systems with modes that scale with different dynamic critical exponents have been found in theories of the quantum nematic transition in 2d metals [4–6]. Finally, although we focused on spin 1, the physics we discussed applies to other quantum spin chains, such as spin 1/2 ones, even without an RK structure [23]. We thus see the emergence of a unified picture for a broad class of quantum critical systems with non-trivial dynamics. An important missing element in both 1d and 2d is a field theory description, although our present analysis might help guide the search. This program will also shed light on the non-equilibrium dynamics of classical systems via the exact map of Henley discussed above [11].

ACKNOWLEDGMENTS

We thank A. Ludwig, R. Movassagh, S. Sachdev, M. Stoudenmire and X. Yu for useful discussions. XC was supported by a postdoctoral fellowship from the Gordon and Betty Moore Foundation, under the EPiQS initiative, Grant GBMF4304, at the Kavli Institute for The-

oretical Physics. This work was supported in part by the US National Science Foundation through grant DMR 1408713 at the University of Illinois (EF). WWK was funded by a Discovery Grant from NSERC, and by a

Canada Research Chair. The DMRG simulations were performed using the ITensor package (v2). We acknowledge support from the Center for Scientific Computing from the CNSI, MRL: an NSF MRSEC (DMR-1121053).

[1] John A. Hertz, “Quantum critical phenomena,” *Phys. Rev. B* **14**, 1165–1184 (1976).

[2] A. J. Millis, “Effect of a nonzero temperature on quantum critical points in itinerant fermion systems,” *Phys. Rev. B* **48**, 7183–7196 (1993).

[3] S. Sachdev, *Quantum Phase Transitions*, 2nd ed. (Cambridge University Press, Cambridge, UK, 2011).

[4] Vadim Oganesyan, Steven A. Kivelson, and Eduardo Fradkin, “Quantum Theory of a Nematic Fermi Fluid,” *Phys. Rev. B* **64**, 195109 (2001).

[5] T. Meng, A. Rosch, and M. Garst, “Quantum criticality with multiple dynamics,” *Phys. Rev. B* **86**, 125107 (2012), arXiv:1205.3400 [cond-mat.str-el].

[6] Samuel Lederer, Yoni Schattner, Erez Berg, and Steven A. Kivelson, “Superconductivity and non-Fermi liquid behavior near a nematic quantum critical point,” (2016), arXiv:1612.01542.

[7] Philippe Di Francesco, Pierre Mathieu, and David Sénéchal, *Conformal Field Theory* (Springer-Verlag, New York, 1996).

[8] A. Lucas, S. Gazit, D. Podolsky, and W. Witczak-Krempa, “Dynamical Response near Quantum Critical Points,” *Physical Review Letters* **118**, 056601 (2017), arXiv:1608.02586 [cond-mat.str-el].

[9] S. Bravyi, L. Caha, R. Movassagh, D. Nagaj, and P. W. Shor, “Criticality without Frustration for Quantum Spin-1 Chains,” *Physical Review Letters* **109**, 207202 (2012), arXiv:1203.5801 [quant-ph].

[10] Daniel S. Rokhsar and Steven A. Kivelson, “Superconductivity and the quantum hard-core dimer gas,” *Phys. Rev. Lett.* **61**, 2376–2379 (1988).

[11] C. L. Henley, “From classical to quantum dynamics at Rokhsar Kivelson points,” *Journal of Physics Condensed Matter* **16**, S891–S898 (2004), cond-mat/0311345.

[12] Eddy Ardonne, Paul Fendley, and Eduardo Fradkin, “Topological order and conformal quantum critical points,” *Annals of Physics* **310**, 493 (2004).

[13] S. V. Isakov, P. Fendley, A. W. W. Ludwig, S. Trebst, and M. Troyer, “Dynamics at and near conformal quantum critical points,” *Phys. Rev. B* **83**, 125114 (2011), arXiv:1012.3806 [cond-mat.str-el].

[14] See Supplemental Material.

[15] R. Movassagh, “Entanglement and correlation functions of the quantum Motzkin spin-chain,” *Journal of Mathematical Physics* **58**, 031901 (2017), arXiv:1602.07761 [quant-ph].

[16] Ramis Movassagh and Peter W. Shor, “Supercritical entanglement in local systems: Counterexample to the area law for quantum matter,” *Proceedings of the National Academy of Sciences* **113**, 13278–13282 (2016), <http://www.pnas.org/content/113/47/13278.full.pdf>.

[17] Z. Zhang, A. Ahmadain, and I. Klich, “Quantum phase transition from bounded to extensive entanglement entropy in a frustration-free spin chain,” ArXiv e-prints (2016), arXiv:1606.07795 [quant-ph].

[18] E. Fradkin, *Field Theories of Condensed Matter Physics*, Field Theories of Condensed Matter Physics (Cambridge University Press, 2013).

[19] S. N. Majumdar, “Brownian functionals in physics and computer science,” *Curr. Sci.* **88**, 2076–2092 (2005), cond-mat/0510064.

[20] L. Dell’Anna, O. Salberger, L. Barbiero, A. Trombettoni, and V. E. Korepin, “Violation of cluster decomposition and absence of light cones in local integer and half-integer spin chains,” *Phys. Rev. B* **94**, 155140 (2016), arXiv:1604.08281 [cond-mat.str-el].

[21] E. Fradkin and J. E. Moore, “Entanglement Entropy of 2D Conformal Quantum Critical Points: Hearing the Shape of a Quantum Drum,” *Physical Review Letters* **97**, 050404 (2006), cond-mat/0605683.

[22] M. M. Wolf, F. Verstraete, M. B. Hastings, and J. I. Cirac, “Area Laws in Quantum Systems: Mutual Information and Correlations,” *Physical Review Letters* **100**, 070502 (2008), arXiv:0704.3906 [quant-ph].

[23] Xiao Chen, Eduardo Fradkin, and William Witczak-Krempa, “Gapless quantum spin chains: multiple dynamics and conformal wavefunctions,” *Journal of Physics A: Mathematical and Theoretical* **50**, 464002 (2017), arXiv:1707.02317 [cond-mat.str-el].

[24] Pasquale Calabrese, John Cardy, and Erik Tonni, “Entanglement entropy of two disjoint intervals in conformal field theory II,” *Journal of Statistical Mechanics: Theory and Experiment* **2011**, P01021 (2011).

[25] D. Gosset and E. Mozgunov, “Local gap threshold for frustration-free spin systems,” *Journal of Mathematical Physics* **57**, 091901 (2016), arXiv:1512.00088 [quant-ph].

[26] R. Moessner, S. L. Sondhi, and Eduardo Fradkin, “Short-ranged resonating valence bond physics, quantum dimer models, and Ising gauge theories,” *Phys. Rev. B* **65**, 024504 (2001).

[27] Claudio Castelnovo, Claudio Chamon, Christopher Mudry, and Pierre Pujol, “From quantum mechanics to classical statistical physics: Generalized Rokhsar-Kivelson Hamiltonians and the Stochastic Matrix Form decomposition,” *Annals of Physics* **318**, 316–344 (2005).

[28] P. C. Hohenberg and B. I. Halperin, “Theory of dynamic critical phenomena,” *Rev. Mod. Phys.* **49**, 435–479 (1977).

[29] M. D. Grynberg, “Revisiting Kawasaki dynamics in one dimension,” *Phys. Rev. E* **82**, 051121 (2010), arXiv:1009.4511 [cond-mat.stat-mech].

[30] Robert Cordery, Sanjoy Sarker, and Jan Tobochnik, “Physics of the dynamical critical exponent in one dimension,” *Phys. Rev. B* **24**, 5402–5403 (1981).

[31] P. Calabrese, J. Cardy, and E. Tonni, “Entanglement Negativity in Quantum Field Theory,” *Physical Review Letters* **109**, 130502 (2012), arXiv:1206.3092 [cond-mat.stat-mech].

Supplemental Material

Appendix A: Generalized Motzkin Hamiltonian in spin language

The full Hamiltonian for a chain of N sites reads

$$H = H_{\text{bulk}}(c) + H_{\text{bdy}} \quad (\text{A1})$$

where the bulk Hamiltonian is a sum of D, U, V projectors:

$$\begin{aligned} H_{\text{bulk}}(c) &= \sum_{i=1}^{N-1} \Pi_{i,i+1} \quad (\text{A2}) \\ &= \sum_{i=1}^{N-1} |D\rangle_{i,i+1}\langle D| + |U\rangle_{i,i+1}\langle U| + c|V\rangle_{i,i+1}\langle V| \end{aligned}$$

with $|D\rangle = \frac{1}{\sqrt{2}}(|0d\rangle - |d0\rangle)$, $|U\rangle = \frac{1}{\sqrt{2}}(|0u\rangle - |u0\rangle)$, $|V\rangle = \frac{1}{\sqrt{2}}(|00\rangle - |ud\rangle)$ and the parameter $c \geq 0$. Here, $u, d, 0$ label the S^z eigenstates. These projectors can be written in terms of spin operators:

$$\begin{aligned} 4|D\rangle_{1,2}\langle D| &= S_1^z + S_2^z + (S_1^z)^2 + (S_2^z)^2 \\ &\quad - (S_1^z)^2 S_2^z - S_1^z (S_2^z)^2 - 2(S_1^z)^2 (S_2^z)^2 \\ &\quad - S_1^- S_1^z S_2^z S_2^+ - S_1^z S_1^+ S_2^- S_2^z \quad (\text{A3}) \end{aligned}$$

$$\begin{aligned} 4|U\rangle_{1,2}\langle U| &= -S_1^z - S_2^z + (S_1^z)^2 + (S_2^z)^2 \\ &\quad + (S_1^z)^2 S_2^z + S_1^z (S_2^z)^2 - 2(S_1^z)^2 (S_2^z)^2 \\ &\quad - S_1^+ S_1^z S_2^z S_2^- - S_1^z S_1^- S_2^+ S_2^z \quad (\text{A4}) \end{aligned}$$

$$\begin{aligned} 4|V\rangle_{1,2}\langle V| &= 2 - 2(S_2^z)^2 - 2(S_1^z)^2 - \frac{1}{2}S_1^z S_2^z \\ &\quad - \frac{1}{2}(S_1^z)^2 S_2^z + \frac{1}{2}S_1^z (S_2^z)^2 + \frac{5}{2}(S_1^z)^2 (S_2^z)^2 \\ &\quad + S_1^- S_1^z S_2^+ S_2^z + S_1^z S_1^+ S_2^z S_2^- \quad (\text{A5}) \end{aligned}$$

where the raising/lowering operators are defined as usual:

$$S^\pm = S^x \pm iS^y \quad (\text{A6})$$

with the standard commutation relations

$$[S^\pm, S^z] = \mp S^\pm, \quad [S^+, S^-] = 2S^z \quad (\text{A7})$$

At $c = 1$, the spin representation was also discussed in Ref. 15. We note that some terms in the U, D, V projectors involve 3 spin operators. These can be converted to a 4-spin interaction using the above commutation relations. We thus see that the Hamiltonian is of the bilinear-biquadratic form, $\sum_j (A_{ab} S_j^a S_{j+1}^b + B_{ab;cd} S_j^a S_j^b S_{j+1}^c S_{j+1}^d)$. This representation is convenient for the DMRG calculations.

One can verify that neighboring $\Pi_{i,i+1}$ operators do

not commute, e.g.

$$[\Pi_{12}, \Pi_{23}] \neq 0 \quad (\text{A8})$$

However, the Hamiltonian is “frustration-free” in the quantum information sense of the word, because all the $\Pi_{i,i+1}$ have at least one common zero-eigenvalue eigenstate:

$$\Pi_{i,i+1} |\Psi_0\rangle = 0 \quad (\text{A9})$$

It can be easily verified that the bulk Hamiltonian has a global $U(1)$ symmetry, i.e. we have the following commutation relation:

$$\left[\sum_i S_i^z, H_{\text{bulk}} \right] = 0 \quad (\text{A10})$$

The boundary term is

$$H_{\text{bdy}} = H_{\text{bdy}}^{i=1} + H_{\text{bdy}}^{i=N} \quad (\text{A11})$$

$$= \frac{1}{2}S_1^z(S_1^z - 1) + \frac{1}{2}S_N^z(S_N^z + 1) \quad (\text{A12})$$

It is important to realize that H_{bdy} does not commute with the bulk Hamiltonian:

$$[H_{\text{bdy}}, H_{\text{bulk}}] \neq 0 \quad (\text{A13})$$

The boundary term commutes with the symmetry generator $\sum_{i=1}^N S_i^z$, implying that the full Hamiltonian is symmetric:

$$\left[\sum_i S_i^z, H \right] = 0 \quad (\text{A14})$$

Appendix B: Field theory calculations

For the groundstate wavefunction defined in Eq.(5) of the main text, if we change $\phi \rightarrow X$ and $x \rightarrow \tau$, we recognize that it is the path integral for a quantum mechanical particle in imaginary time τ . The particle’s Hamiltonian in the position basis is ($\hbar = 1$)

$$\hat{H}_1 = -\frac{1}{4\kappa} \frac{d^2}{dX^2} + V(X) \quad (\text{B1})$$

with mass $m = 2\kappa$. The potential is:

$$V(X < 0) = \infty, \quad V(X \geq 0) = 0 \quad (\text{B2})$$

The infinite wall for $X < 0$ prevents the particle from penetrating the negative half-line, i.e. it enforces the “orbifold condition” on the ϕ field. The eigenstates of \hat{H}_1 are forced to vanish beyond the wall $X < 0$, but are otherwise eigenstates of the free particle Hamiltonian when $X > 0$. We thus find the eigenfunctions

$\psi_k(X) = \sqrt{2/\pi} \sin(kX)$ for $X > 0$ and zero when $X < 0$, with $k \geq 0$ being a continuous wave number. The corresponding energies are $E_k = k^2/(2m) = k^2/(4\kappa)$.

Based on this complete set of eigenfunctions, we can evaluate the propagator G :

$$\begin{aligned} G(X_f, \tau_f; X_i, \tau_i) &\equiv \langle X_f | e^{-(\tau_f - \tau_i)\hat{H}_1} | X_i \rangle \\ &= \int_0^\infty dk \langle X_f | e^{-(\tau_f - \tau_i)\hat{H}_1} | \psi_k \rangle \langle \psi_k | X_i \rangle \\ &= \sqrt{\frac{\kappa}{\pi(\tau_f - \tau_i)}} \left[e^{-\frac{\kappa(X_f - X_i)^2}{(\tau_f - \tau_i)}} - e^{-\frac{\kappa(X_f + X_i)^2}{(\tau_f - \tau_i)}} \right] \quad (\text{B3}) \end{aligned}$$

Notice there's no i in the evolution operator because we work in Euclidean time. From the propagator G , we can further calculate the probability distribution function for the particle being at X at time τ :

$$f(X, \tau) = \frac{\langle X_f, \tau_f | X, \tau \rangle \langle X, \tau | X_i, \tau_i \rangle}{\langle X_f, \tau_f | X_i, \tau_i \rangle} \quad (\text{B4})$$

Going back to the original wavefunction, this gives the probability function for being at height ϕ at position x . We impose the boundary conditions

$$X_i = X_f = \delta, \quad \tau_i = 0, \quad \tau_f = L \quad (\text{B5})$$

where we have introduced a regulator $\delta = 0^+$. Using Eq.(B3), we then find for $\phi \geq 0$

$$f(\phi, x) = \frac{1}{2\sqrt{\pi}} \left(\frac{4\kappa L}{(L-x)x} \right)^{3/2} \phi^2 \exp \left[\frac{-\kappa L \phi^2}{(L-x)x} \right] \quad (\text{B6})$$

where we have changed notation back, i.e., $X \rightarrow \phi$ and $\tau \rightarrow x$, as suitable for the height quantum field ϕ . We note that the factor of ϕ^2 results from the constraint $\phi > 0$, which makes the distribution function f deviate from a Gaussian. One can verify that the probability distribution is properly normalized: $\int_0^\infty d\phi f(\phi, x) = 1$.

Using the probability distribution Eq.(B6), we can evaluate the Rényi entanglement entropies for region A being the interval $[0, L_A]$, as given in Eq.(7) of the main text. The reduced density matrix for region A is

$$\rho_A = \sqrt{\epsilon} f(\sqrt{\epsilon}\varphi, L_A) |\varphi\rangle\langle\varphi| \quad (\text{B7})$$

where $\varphi = \phi/\sqrt{\epsilon}$ is the dimensionless height variable, normalized by the short distance cutoff ϵ . For general n , the Rényi entropy is

$$\begin{aligned} S_n &\equiv \frac{1}{1-n} \ln \text{Tr}(\rho_A^n) \\ &= \frac{1}{2} \ln \left[\frac{L_A(L - L_A)}{\epsilon L} \right] + b(n) \quad (\text{B8}) \end{aligned}$$

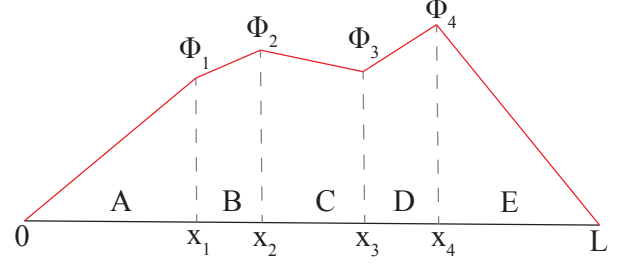


FIG. 3. A configuration with ϕ_i at x_i .

where ϵ is a short distance cutoff and

$$\begin{aligned} b(n) &= -\frac{(2n+1)\ln n + n\ln(\pi/(16\kappa)) + \ln(4\kappa)}{2(1-n)} \\ &\quad + \frac{\ln\Gamma(n + \frac{1}{2})}{1-n} \end{aligned} \quad (\text{B9})$$

The leading log term for S_n agrees with the result for the Motzkin spin Hamiltonian [9, 15]. The second term also agrees with the lattice result if we choose $\kappa = 3/4$, which is the value derived in the main text. In the limit $L_A \ll L$, we obtain:

$$S_n = \frac{1}{2} \ln \left(\frac{L_A}{\epsilon} \right) + \dots \quad (\text{B10})$$

Thus the EE has a logarithmic dependence on L_A , suggesting that the groundstate is highly entangled [9].

1. Mutual information

We consider two short intervals B and D (Fig. 3) deep inside the bulk and compute the mutual information between them. If $L_B, L_C, L_D \ll L_A, L_E$, the probability for the height field ϕ in region B, C, D to approach zero is exponentially small. Therefore the physics in the bulk region can be essentially described by the unconstrained $z = 2$ boson.

For the unconstrained boson, the probability distribution for the height field is simply a Gaussian distribution and it is easy to show that reduced density matrix for region $B \cup D$ depends only on $\phi_B \equiv \phi_2 - \phi_1$, $\phi_D \equiv \phi_3 - \phi_4$, where $\phi_i = \phi(x_i)$, and is equal to

$$\begin{aligned} \rho_{B \cup D} &\sim \int \mathcal{D}\phi_B \mathcal{D}\phi_D \\ &\times e^{-\frac{\kappa L_D(L - L_D)\phi_B^2 + \kappa L_B(L - L_B)\phi_D^2 - 2\kappa L_B L_D \phi_B \phi_D}{L_B L_D(L - L_B - L_D)}} \\ &\times |\phi_B, \phi_D\rangle\langle\phi_B, \phi_D| \quad (\text{B11}) \end{aligned}$$

Therefore the Rényi entropy for $B \cup D$ is

$$S_n(B \cup D) = \frac{1}{2} \ln \left(\frac{L_B L_D}{\epsilon^2} \right) + \frac{1}{2} \ln \frac{L - L_B - L_D}{L} + \ln(\pi/\kappa) - \frac{1}{(1-n)} \ln n \quad (\text{B12})$$

Similarly, we can also calculate EE for each interval and we have

$$\begin{aligned} S_n(B) &= \frac{1}{2} \ln(\pi/\kappa) + \frac{1}{2} \ln \frac{L_B}{\epsilon} + \frac{1}{2} \ln \frac{L - L_B}{L} - \frac{1}{2(1-n)} \ln n \\ S_n(D) &= \frac{1}{2} \ln(\pi/\kappa) + \frac{1}{2} \ln \frac{L_D}{\epsilon} + \frac{1}{2} \ln \frac{L - L_D}{L} - \frac{1}{2(1-n)} \ln n \end{aligned} \quad (\text{B13})$$

The mutual information between B and D is

$$\begin{aligned} I_n(B, D) &= S_n(B) + S_n(D) - S_n(B \cup D) \\ &= \frac{1}{2} \ln \frac{(L - L_B)(L - L_D)}{(L - L_B - L_D)L} \end{aligned} \quad (\text{B14})$$

We first note that $I_n(B, D)$ does not depend on the Rényi index. In the limit $L_B, L_D \ll L$, the mutual information vanishes.

2. Logarithmic negativity

We now turn to the logarithmic negativity, which detects the entanglement between 2 disjoint regions and is defined as

$$\mathcal{N} = \ln \|\rho_{B \cup D}^{T_D}\|, \quad (\text{B15})$$

where $\rho_{B \cup D}^{T_D}$ denotes the partial transpose of the reduced density matrix $\rho_{B \cup D}$ with respect to region D . $\|\mathcal{O}\|$ is the sum of the absolute value of the eigenvalues of \mathcal{O} . For 2 intervals deep in the bulk, $\rho_{B \cup D}$ given in Eq.(B11) is diagonal and invariant under the partial transpose for ϕ_D , in contrast to the generic case. Thus $\mathcal{N} = \ln \text{tr}(\rho_{B \cup D}) = 0$, further supporting the claim that the Motzkin wavefunction is less entangled than the groundstate of a CFT [31].

Appendix C: DMRG calculations

We have numerically calculated the energy gap between the groundstate and the lowest energy excited states ΔE by using both exact diagonalization (ED) and the density matrix renormalization group (DMRG). The ED method is used for small systems $N \leq 10$ as a benchmark, and we perform large-scale DMRG calculations using the open-source C++ library ITensor.

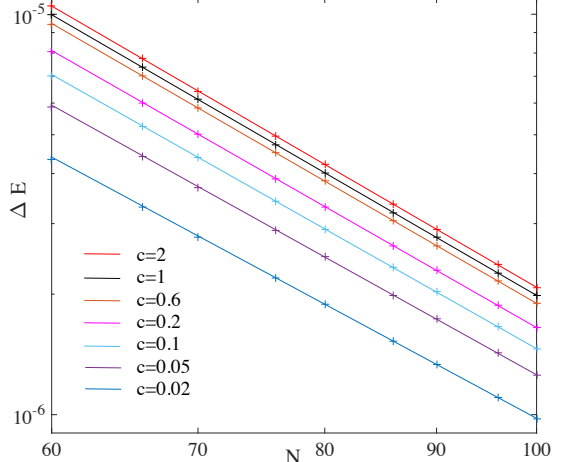


FIG. 4. Log-log plot of the energy gap ΔE versus system size N for various c . The lines are fits to $\Delta E \propto N^{-z}$ using the data points $N \geq 80$.

For the generalized Motzkin model, ΔE scales as $1/N^z$ for sufficiently large N . According to the previous ED result on small systems at $c = 1$, the dynamical exponent z is large and close to 3 [9]. Meanwhile, this model is spin $S = 1$. Both these factors make the DMRG more difficult, especially if high precision is required. As a first step, we compare the groundstate energy and the von Neumann EE obtained via DMRG with the analytical results and find that they agree precisely. Then, in order to calculate the lowest excitations, which is doubly degenerate and has $S_{\text{tot}}^z = \pm 1$, a large number of sweeps is used to ensure that the gap is well converged (the energy deviation for the last two sweeps is less than 10^{-12}).

We calculate the energy for the lowest excited state in the $S_{\text{tot}}^z = 1$ sector. We show the energy gap ΔE between the groundstate and this state in Fig. 4 as a function of system size. We fit $\Delta E \propto 1/N^z$ using the data points in the range $80 \leq N \leq 100$ in order to minimize finite-size effects. When $N \geq 80$, ΔE is less than 10^{-5} and decreases as c decreases, which makes the small c simulations more difficult.

The dynamical exponent z is obtained by finite size scaling with N from 80 to 100, with the detail is shown in Table I. Moreover, we calculate the lowest excited state with $S_{\text{tot}}^z = 0$ and show the dynamical exponent z_0 in Table I. We consider smaller system sizes $52 \leq N \leq 80$ because the calculation of the excited state in the same spin sector as the groundstate is time-consuming. In Fig. 5, we show the size dependence of the gap in the $S_{\text{tot}}^z = 2$ sector. The fit yields a dynamical exponent of $z' = 3.18$, which is very close to the value obtained in the $S_{\text{tot}}^z = 1$ sector, $z = 3.16$. This suggests that both sectors have the same dynamical exponent.

In Fig. 6, we show an alternate method to estimate z in the thermodynamic limit. For 2 consecutive values of N , $N_1 < N_2$, we evaluate the finite size exponent at the

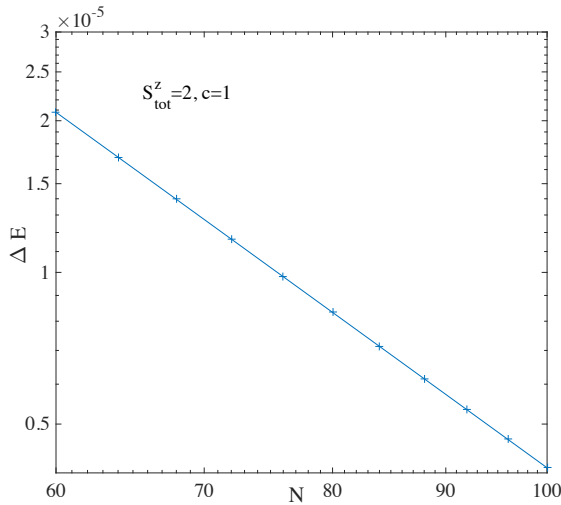


FIG. 5. Log-log plot of the energy gap ΔE in the $S_{\text{tot}}^z = 2$ sector versus system size N at $c = 1$. The line is a fit to $\Delta E \propto N^{-z'}$ using the data points $N \geq 80$. The fit yields $z' = 3.18$.

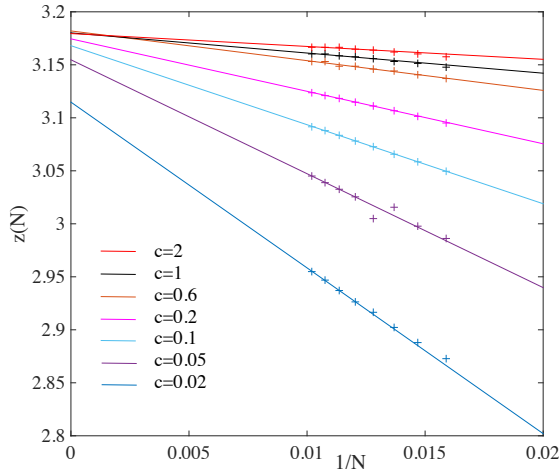


FIG. 6. Dynamical exponent $z(N)$ versus $1/N$ for various c . The crosspoint with vertical axis is $z(\infty)$.

midpoint:

$$z\left(\frac{N_1 + N_2}{2}\right) = -\frac{\ln(\Delta E_2/\Delta E_1)}{\ln(N_2/N_1)} \quad (\text{C1})$$

The dependence of $z(N)$ on N is shown in Fig. 6 for different values of the coupling c . We notice that the variation of $z(N)$ with N is small when $c \geq 0.6$. As we decrease c , finite size effects for $z(N)$ become larger and we notice that $z(N)$ roughly scales as $1/N$. In order to get an estimate for z in the thermodynamic limit, we use a $1/N$ fit for the 4 largest N points ($N > 80$) to extract $z(N \rightarrow \infty)$. We compare the corresponding results with z obtained from the fits described above in Table I. It is important to emphasize that the $1/N$ extrapolation for

c	z	$z(\infty)$	z_0	$z_0(\infty)$
0	2		2	
0.02	2.94	3.11		
0.05	3.03	3.15		
0.1	3.08	3.17	2.63	2.70
0.2	3.12	3.17		
0.4			2.70	2.70
0.6	3.15	3.18		
1	3.16	3.18	2.71	2.70
2	3.17	3.18		

TABLE I. The dynamical exponents of the generalized Motzkin spin chain as a function of c , both in the $S_{\text{tot}}^z = 1$ and $S_{\text{tot}}^z = 0$ sectors. The lowest lying excited state has $S_{\text{tot}}^z = 1$. The $z(\infty)$ results are obtained using the extrapolation in Fig. 6.

$z(N)$ may not be accurate at $c < 0.6$, and is only an estimate for the true z . For instance, the slope could change at larger N , or deviate from $1/N$ scaling.